Volodymyr Babizhetskyy*, Jürgen Köhler, Yuriy Tyvanchuk and Chong Zheng

A new ternary silicide $GdFe_{1-x}Si_2$ ($x = 0.32$): preparation, crystal and electronic structure

https://doi.org/10.1515/znb-2019-0200
Received November 29, 2019; accepted December 6, 2019

Abstract: The title compound was prepared from the elements by arc-melting. The crystal structure was investigated by means of single-crystal X-ray diffraction. It crystallizes in the $TbFeSi_2$ structure type, orthorhombic space group *Cmmm*, $a = 4.0496(8)$, $b = 16.416(2)$, $c = 3.9527(6)$ Å, $Z = 4$, $R1 = 0.041$, $wR2 = 0.11$ for 207 unique reflections with $I_o > 2\,\sigma(I_o)$ and 19 refined parameters. The Fe position is not fully occupied and the refinement results in a composition $GdFe_{0.68}Si_2$ in agreement with a chemical analysis. The structure consists of zig-zag chains of Si(1) atoms which are terminally bound to additional Si(2) atoms. For an ordered variant $GdFe_{0.5}Si_2$ the Zintl concept can be applied which results in formal oxidation states $Gd^{3+}(Fe^{2+})_{0.5}Si(1)^{1-}Si(2)^{3-}$. The electronic structure of this variant $GdFe_{0.5}Si_2$ was analyzed using the tight-binding LMTO method and the results confirm the simple bonding picture.

Keywords: crystal structure; electronic structure; gadolinium iron silicide; $TbFeSi_2$ structure type.

Dedicated to: Professor Arndt Simon on the occasion of his 80th birthday.

1 Introduction

Several ternary compounds with the approximate composition $RT_{1-x}Si_2$ (R = rare earth, T = transition element) have been reported during the last decades. Their crystal structures are characterized by a stacking of $BaAl_4$ and AlB_2 related slabs. Most compounds with T = Co–Cu crystallize in the $CeNiSi_2$-type structure [1]. Different structures were found for the $RT_{1-x}Si_2$ compositions. The early rare earth manganese $RMn_{1-x}Si_2$ (R = La–Sm) and iron $RFe_{1-x}Si_2$ (R = La–Tb) silicides crystallize in the $LaMnSi_2$-type structure [2–4], a structure closely related to the $CeNiSi_2$-type structure, and they are characterized by a site exchange between the transition-metal and the main-group elements within the $BaAl_4$ block. The atomic positions in the $LaMnSi_2$-type structure correspond to those in the $TbFeSi_2$-type structure earlier discovered by Yarovets and Gorelenko [5]. We use the earlier discovered type of structure for our denomination in the text. Investigations in quaternary systems *R*-*T*-*T*′-*X* led to the characterization of new isotypic representatives of the $TbFeSi_2$-type structure with the composition $RTT'_{0.5}X_{1.5}$ (R = La–Sm; T = Mn, Co, Rh, Re; T' = Cu, Ni, Pd, Pt; X = Si, Ge) [6–11]. All compounds show the T' substitution in the AlB_2 slabs.

Paccard et al. [9] re-investigated $TbFeSi_2$ first discovered by Yarovets and Gorelenko [5]. From single-crystal X-ray diffraction data of the $RFeSi_2$ (R = Ho, Tb, Dy) compounds, they concluded that these phases are non-stoichiometric and should rather be named as $RFe_{0.5}Si_2$ because an iron non-stoichiometry is evident. Due to the very small difference between the X-ray scattering factors for a fully occupied silicon site or a half-occupied iron site, this study does not clearly distinguish between the two site exchange variants, i.e. the $TbFeSi_2$ and $CeNiSi_2$ structure types. Norlidah et al. [10] using neutron diffraction and ^{57}Fe Mössbauer spectroscopy for $HoFe_{0.5}Si_2$ have suggested that this compound crystallizes in the $CeNiSi_2$-type structure and partially removed the uncertainties outlined by Paccard et al. [9] concerning the localization of the transition metal in the heavy rare earth $RFe_{1-x}Si_2$ compounds (R = Tb, Dy, Ho, Er, Lu). The $TbFeSi_2$ structure type also has quaternary representatives in the *R*-Mn-*T*-Si systems: $RMnPd_{0.5}Si_{1.5}$ (R = La, Ce), $RMnPt_{0.5}Si_{1.5}$ (R = La, Ce, Pr), and $RMnCu_{0.5}Si_{1.5}$ (R = La, Ce–Nd) [11].

For the $RT_{1-x}X_2$ compounds with the $CeNiSi_2$-type structure, the non-stoichiometry increases with the period number of the tetrele element with the same rare earth and transition metal element i.e.: $HoFe_{0.5}Si_2$, $HoFe_{0.38}Ge_2$, and $HoFe_{0.14}Sn_2$ [12]. By fixing the rare earth and tetrele elements, the transition metal content increases with the group number of the transition metal i.e.: $LuFe_{0.3}Si_2$ [13], $LuCo_{0.85}Si_2$ [14], and $LuNiSi_2$ [1].

***Corresponding author: Volodymyr Babizhetskyy,** Faculty of Chemistry, Ivan Franko National University of Lviv, Kyryla i Mefodiya Street 6, UA-79005, Lviv, Ukraine,
e-mail: v.babizhetskyy@googlemail.com
Jürgen Köhler: Max-Planck-Institut für Festkörperforschung, Heisenbergstrasse 1, Postfach 800665, D-70569, Stuttgart, Germany
Yuriy Tyvanchuk: Faculty of Chemistry, Ivan Franko National University of Lviv, Kyryla i Mefodiya Street 6, UA-79005, Lviv, Ukraine
Chong Zheng: Department of Chemistry and Biochemistry, Northern Illinois University, DeKalb, IL 60115, USA

Finally, the RRuSi$_2$-type compounds (R = La, Ce, Nd, Sm, Gd, Tb) and the stoichiometric RFeSi$_2$-type compounds (R = Nd, Sm, Gd, Tb) adopt the NdRuSi$_2$-type structure, a monoclinic variant of the CeNiSi$_2$ type [3, 15, 16]. The NdRuSi$_2$-type structure family includes the non-stoichiometric $CeNi_{1-x}Si_2$ and $CeNi_{1-x}Si_{2+x}$ structures with vacancies or mixed occupations on the transition metal sites [14]. The compounds $CeRh_{1-x}Ge_{2+x}$ ($x = 0.325$) crystallize in a primitive orthorhombic cell with disordered substitution on half of the transition-metal sites [17], while the $TmLi_{1-x}Ge_2$ ($x = 0.5$) structure is another monoclinically distorted variant [18].

In the course of systematic phase-analytical studies of the Gd–Fe–Si system we have obtained new phases. A closer inspection of the new compound $GeFe_{1-x}Si_2$ became the subject of the present work.

2 Experimental

2.1 Synthesis

Polycrystalline samples of different compositions GdFeSi$_2$, $GdFe_{0.8}Si_2$, $GdFe_{0.5}Si_2$ and $GdFe_{0.4}Si_2$ were prepared from the commercially available pure elements: gadolinium metal with a claimed purity of 99.99 at.%, Alfa-Aesar, Johnson Matthey Company, sublimed bulk pieces; silicon as powder, purity >99.99 at.%, H. C. Starck, Germany; iron powder, purity 99.98 at.%, Fluka Chemicals. Suitable amounts of powders and freshly filed chips of the rare earth metal were mixed together and pressed into pellets. Arc-melting of the samples (1.00 g each) was performed on a water-cooled copper hearth under a purified argon atmosphere with Ti as the getter. To ensure homogeneity, the samples were turned over and re-melted three times. Weight losses were generally smaller than 0.5%. For further heat treatments, the pellets were wrapped in tantalum foil, sealed in evacuated quartz tubes, annealed at $T = 800$°C for 1 month and subsequently quenched by submerging the tubes in cold water. Single crystals of the new gadolinium iron silicide, having a metallic luster and being unreactive towards air, were isolated by crushing the solidified samples.

2.2 Microprobe analysis

For metallographic inspection and for complementary qualitative phase analysis, energy dispersive X-ray spectroscopy (EDX) was employed. The samples were embedded in Wood's metal (melting point of 75°C, Fluka Chemie, Switzerland). The embedded samples were polished on a nylon cloth using chromium oxide (Bühler Isomet) with grain sizes 1–5 μm. Quantitative and qualitative composition analyses of the polished samples were performed by energy-dispersive X-ray spectroscopy (EDX) on a scanning electron microscope TESCAN 5130 MM with an Oxford Si-detector. From the EDX analysis of the arc-melted sample $GdFe_{0.4}Si_2$ the composition $Gd_{26.2(3)}Fe_{18.0(3)}Si_{55.6(3)}$ was deduced. For the chemical microprobe, the polishing procedure had to be performed or repeated just before the measurements. The surface of the phases in the Gd–Fe–Si system appears to be quite stable in air. Metallographic investigation, X-ray powder diffraction and EDX analyses revealed the presence of the phases $Gd_2Fe_3Si_5$ [19] and $Gd_{1.2}Fe_4Si_9$ [20] besides the new compound $GdFe_{1-x}Si_2$ ($x = 0.32$) (Fig. 1). After the annealing procedure, only $Gd_2Fe_3Si_5$ and GdSi$_2$ [21] were found in the $GdFe_{0.4}Si_2$ sample.

2.3 X-ray diffraction and structure refinement

X-ray powder diffraction patterns were obtained on a powder diffractometer STOE STADI P with Mo$K\alpha_1$ radiation, using sealed boron glass capillaries. The unit cell parameters were refined with the help of the WinCSD program package [22]. The indexing of the X-ray powder patterns was ensured through intensity calculations taking the atomic positions determined from the single-crystal investigation. The unit cell parameters refined

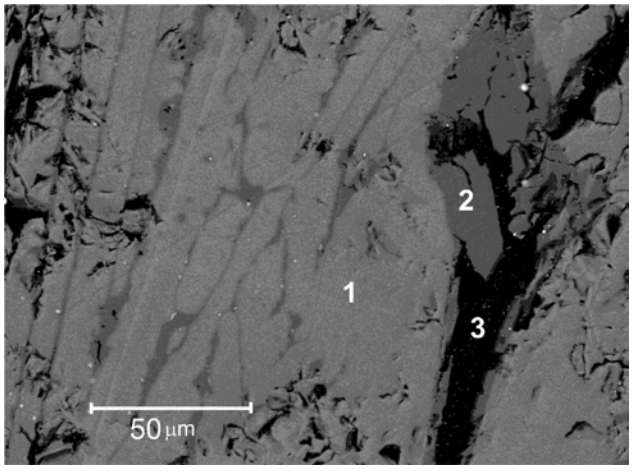

Fig. 1: Backscattered electron image of the arc-cast bulk sample with nominal atomic composition Gd:Fe:Si = 1:0.4:2. (1) $GdFe_{0.68}Si_2$, (2) $Gd_2Fe_3Si_5$, (3) $Gd_{1.2}Fe_4Si_9$.

from X-ray powder data are $a = 4.05781(5)$, $b = 16.424(2)$, $c = 3.9652(4)$ Å. The small difference between the lattice parameters determined from single-crystal and powder diffraction, respectively, are quite normal.

Small and irregularly platelet-shaped single crystals for X-ray investigation were selected from the crushed arc-melted sample of $GdFe_{0.4}Si_2$. These crystals were first examined by the Buerger precession method in order to establish their suitability for intensity data collection. After the X-ray data collection on a STOE IPDS II image plate diffractometer, an EDX analysis of the single crystal revealed the composition $Gd_{27.3(3)}Fe_{19.1(3)}Si_{53.6(3)}$, which is in good agreement with the results obtained from the bulk sample, and the small difference indicates surface irregularities of single crystals.

Single-crystal X-ray data of $GdFe_{1-x}Si_2$ ($x = 0.32$) was collected at room temperature on a Stoe IPDS II image plate diffractometer with monochromatized Mo$K\alpha$ radiation in oscillation mode. The lattice parameters were determined from 3150 reflections in the region 4.8–58.98°. All relevant details concerning the data collection are listed in Table 1.

Table 1: Crystallographic data for $GdFe_{1-x}Si_2$ $x = 0.32$.

Empirical formula	$GdFe_{0.68}Si_2$
Crystal system:	Orthorhombic
Space group	*Cmmm* (No. 65)
Pearson symbol	oC16
Lattice parameters	
a, Å	4.0496(8)
b, Å	16.416(2)
c, Å	3.9527(6)
Unit cell volume *V*, Å^3	262.77(7)
Calculated density, g cm^{-3}	6.81
Absorption coefficient, mm^{-1}	31.1
Crystal size, mm^3	$0.12 \times 0.09 \times 0.02$
Radiation/wavelength, Å	Mo$K\alpha$/0.71069
Diffractometer	STOE IPDS II
Refined parameters	19
Refinement	F^2
$2\theta_{max}$, deg/$(\sin\theta/\lambda)_{max}$, Å^{-1}	58.21/0.684
hkl indices range	$-5 \le h \le 5$, $-20 \le k \le 22$, $-5 \le l \le 5$
Collected reflections	1223
Independent reflections/R_{int}/R_σ	225/0.102/0.018
Reflections with $I > 2\,\sigma(I)$	207
Final $R1/wR2$ $[I > 2\sigma(I)]$[a,b]	0.041/0.119
Final $R1/wR2$ (all data)[a,b]	0.044/0.111
Extinction coefficient	0.006(2)
Goodness-of-fit[c] on F^2	1.16
Largest diff. hole/peak, e^- Å^{-3}	−3.53/4.14

[a] $R1 = \Sigma\,||F_o| - |F_c||\,/\,\Sigma\,|F_o|$; [b] $wR2 = [\Sigma w(F_o^2 - F_c^2)^2/\Sigma w(F_o^2)^2]^{1/2}$, $w = [\sigma^2(F_o^2) + (0.056P)^2 + 1.938P]^{-1}$, where $P = (\mathrm{Max}(F_o^2, 0) + 2F_c^2)/3$; [c] $\mathrm{GoF} = S = [\Sigma w(F_o^2 - F_c^2)^2/(n_{obs} - n_{param})]^{1/2}$.

The unit cell parameters and extinction rules suggested *Cmmm* as the most appropriate space group. The starting atomic parameters derived *via* Direct Methods using the program Sir 97 [23] were subsequently refined with the program SHELXL-97 [24] (full-matrix least-squares on F^2) with anisotropic displacements parameters for the gadolinium atoms. Only 4 different atomic coordinates were obtained in 4*c* Wyckoff positions, equivalent to those of the $CeNiSi_2$ and $TbFeSi_2$ structure types [1, 5]. First the Gd, Fe and Si atoms were assigned to the 4*c* (0, *y*, 1/4) positions, according to the $CeNiSi_2$ structure. Refinement of the crystal structure with the SHELXL program in anisotropic approximation of the atomic displacement parameters showed non-positive values for the Si1 atoms at $y = 0.7499(3)$. There is a significant residual electron density peak in the difference Fourier map close to the Si1 atom (4.9 e^- Å^{-3}; 0.09 Å). However, the values of the anisotropic atomic displacement U_{iso} for the Fe site with $y = 0.185(3)$ is increased. Refinement of the occupancy (G) for this 4*c* site resulted in $G = 0.612(6)$. The final reliability factor for the $CeNiSi_2$ structure model was $R_1 = 0.049$ ($wR_2 = 0.131$). Exchange of Si1 with Fe atoms led to a site variant of the $CeNiSi_2$ type and considered as the $TbFeSi_2$-type structure. In the next step the Gd, Fe and Si atoms were refined in 4*c* (0 *y* 1/4) positions, according to the $TbFeSi_2$-type structure. The final difference Fourier synthesis was flat and the composition obtained from the structure refinement is in good agreement with the EDX results. Exchange of the Si1 atoms by Fe atoms and refinement of the site occupation for the iron positions led to an improvement of the anisotropic displacement parameters of all atoms with good R values and a satisfactory chemical composition with respect to the EDX analysis ($R_1 = 0.041$; $wR_2 = 0.11$; $S = 1.1$; $Gd_{27.3(3)}Fe_{19.1(3)}Si_{53.6(3)}$). The atomic coordinates and displacement parameters are given in Table 2. Selected interatomic distances and bond angles are reported in Table 3. The program Diamond was used for the drawing of the crystal structure [25].

CCDC 1969021 contains the supplementary crystallographic data for this paper. These data can be obtained free of charge from The Cambridge Crystallographic Data Centre via www.ccdc.cam.ac.uk/data_request/cif.

2.4 Electronic structure calculations

First principles electronic band structure calculations were performed for an ordered variant of $GdFe_{0.5}Si_2$ within the local density approximation [26] using the linear muffin-tin orbital (LMTO) method [27–29] encoded in the TB-LMTO-ASA program [30]. All calculations were

Table 2: Atomic coordinates[a] and displacement parameters[b] (in Å²) for $GdFe_{1-x}Si_2$.

Atom	Occup.	*y*	U_{eq} or U_{iso}	U_{11}	U_{22}	U_{33}
Gd	1.0	0.39603(5)	0.0089(5)	0.0125(7)	0.0084(7)	0.0059(7)
Fe	0.68(2)	0.7501(3)	0.0163(18)	0.024(3)	0.008(2)	0.017(3)
Si1	1.0	0.1850(5)	0.0247(15)	0.015(3)	0.046(4)	0.004(3)
Si2	1.0	0.0411(6)	0.0217(15)	0.030(4)	0.024(3)	0.019(3)

[a]Wyckoff site 4*c* in 0 *y* 1/4. [b]$U_{23} = U_{13} = U_{12} = 0$.

Table 3: Selected interatomic distances *d* (Å) with multiplicities for $GdFe_{1-x}Si_2$.

Atoms	Multiplicity	*d*	Atoms	Multiplicity	*d*
Gd–Gd	2×	4.0496(8)	Fe–Si1	2×	2.290(5)
Gd–Gd	2×	3.9527(7)	Fe–Si1	2×	2.245(5)
Gd–Gd	2×	3.944(1)			
Gd–Si1	1×	3.464(8)	Si1–Gd1	1×	3.464(8)
Gd–Fe	2×	3.137(4)	Si1–Gd1	4×	3.127(4)
Gd–Si2	2×	3.127(8)	Si1–Si2	1×	2.361(3)
Gd–Si1	4×	3.127(4)	Si1–Fe1	2×	2.290(5)
Gd–Fe	2×	3.108(4)	Si1–Fe1	2×	2.245(5)
Gd–Si2	4×	3.011(3)			
			Si2–Gd1	2×	3.127(8)
Fe–Gd	2×	3.137(4)	Si2–Gd1	4×	3.011(3)
Fe–Gd	2×	3.108(4)	Si2–Si2	2×	2.395(8)
Fe–Fe	4×	2.8294(4)	Si2–Si1	1×	2.361(3)

checked for convergence of energies, orbital moments and magnetic moments with respect to the number of *k*-points used in the reciprocal space integrations. Spin orbit coupling was not included and relativistic effects were treated in terms of the scalar relativistic method. Three different classes of empty spheres were used to fill the space in the structure. In our calculations for $GdFe_{0.5}Si_2$ the basis set consisted of Gd 5*d*, Fe 3*s*,*p*,*d* and Si 3*s*,*p* states. The Gd 4*f* states were treated as semicore states. To examine the bonding around the Fermi level between the Si atoms and between the Si atoms and Fe atoms, we performed crystal orbital Hamiltonian population (COHP) analysis [31] which partitions the band structure energy (i.e. the sum of the Kohn-Sham orbital energies) into contributions between pairs of atomic orbitals. The COHP plots are presented under the convention in which positive and negative values refer to bonding and antibonding interactions, respectively.

3 Results and discussion

The crystal structure of $GdFe_{1-x}Si_2$ ($x = 0.32$) is shown in a projection on the (001) plane in Fig. 2. Typical coordination polyhedra (CP) of the various atoms are drawn in Fig. 2a. The gadolinium atoms [$GdGd_6Fe_4Si_{11}$] present a peculiar environment in the form of a hexagonal prism with additional atoms outside the prism faces. Their coordination number (CN) is therefore 21. The gadolinium atoms have close Si neighbors with Gd–Si distances between 3.011(3) and 3.127(4) Å and one Gd–Si distance of 3.464(8) Å (Table 3). The Gd–Fe distances cover the range between 3.108(4) and 3.137(4) Å for the four Fe neighbors of the Gd atom. The orthorhombic prisms with four centered lateral faces [$FeGd_4Fe_4Si_4$] with CN = 12 are the CPs of the iron atoms. They have four close Si atoms with Fe–Si1 distances between 2.245(5) and 2.290(5) Å and four Fe atoms with Fe–Fe distances of 2.8294(4) Å. The silicon atoms have nine metal atom neighbors, forming a trigonal prism with three additional atoms outside the rectangular faces of the prisms: [$Si^1Gd_4Fe_4Si_1$] and [$Si^2Gd_6Si_3$]. Si–Si distances are in the range from 2.361(3) to 2.395(8) Å.

$GdFe_{1-x}Si_2$ ($x = 0.32$) crystallizes in the $TbFeSi_2$-type structure that is built up of an intergrowth of $BaAl_4$ and AlB_2 slabs. This structure type can be considered as a site exchange variant of the $CeNiSi_2$-type structure by interchanging the silicon and the transition metal in the $BaAl_4$ slab (Fig. 2). Both structures types $TbFeSi_2$ and $CeNiSi_2$ are geometrically similar with all atoms in 4*c* Wyckoff positions (space group *Cmcm*). Earlier presented results [2, 13] based on powder X-ray diffraction data for the $RFeSi_2$ compounds (*R* = Y, La–Nd, Tb, Ho, Er, Tm, Lu) were not sufficient for the consideration of structural details. From X-ray diffraction studies on single crystals of the $RFeSi_2$ compounds (*R* = Ho, Tb, Dy), the authors in reference [9] concluded that these phases should rather be named $RFe_{0.5}Si_2$ since an important iron non-stoichiometry is evidenced. The half-occupation of the 4*c* site by an iron atom does not allow to clearly distinguishing between the two site exchange variants. Norlidah et al. [10] on the basis of ^{57}Fe Mössbauer spectroscopy and neutron diffraction data suggested that the RFe_xSi_2 (*R* = Tb, Dy, Ho, Er, Lu) compounds crystallize in the non-stoichiometric $CeNiSi_2$-type structure, although the results of the crystal structure refinement were not presented.

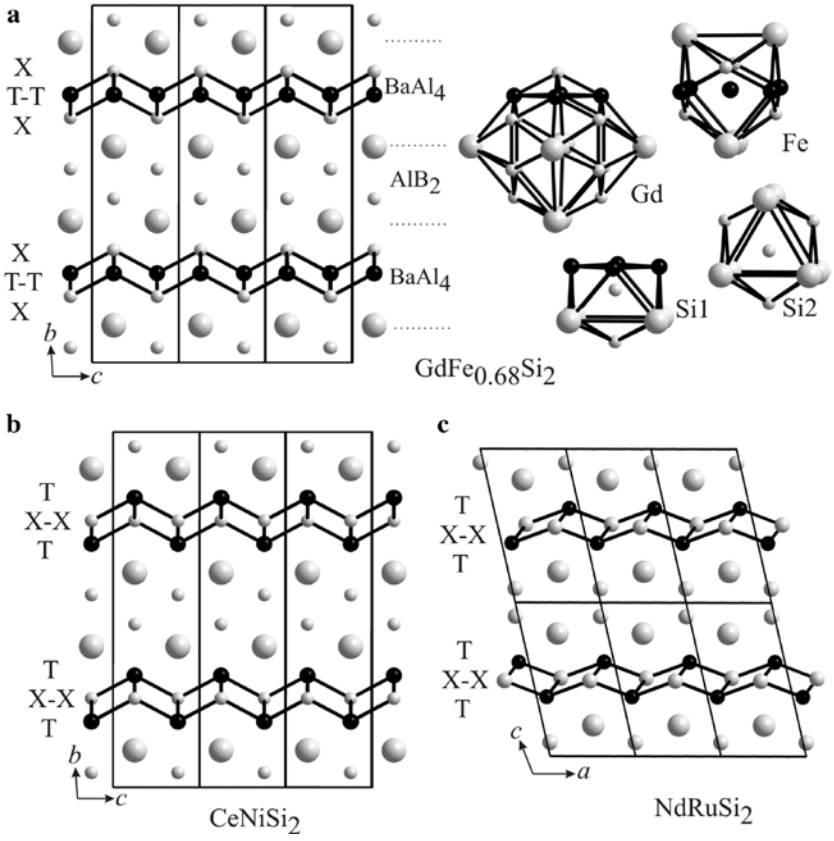

Fig. 2: Structural relationship between (a) $GdFe_{0.68}Si_2$, (b) $CeNiSi_2$ and (c) $NdRuSi_2$. The T_2X_2 layers and coordination polyhedra of related atoms are emphasized. Black and white spheres within the layers correspond to the transition metal and the silicon atoms, respectively.

Several of the ternary compounds with the approximate compositions $RT_{1-x}Si_2$ crystallize in the $CeNiSi_2$, $NdRuSi_2$ and $TbFeSi_2$ types, characterized by different stackings of elementary blocks characteristic of the AlB_2 and $BaAl_4$ crystal structures. The $RT_{1-x}Si_2$ structures are related to one of the well-known $ThCr_2Si_2$ or $CaBe_2Ge_2$ structure types [32, 33]. As the atomic composition is different from 1:2:2, only one part of the structures can be compared. In the $CeNiSi_2$, $NdRuSi_2$ and $TbFeSi_2$ structures the $BaAl_4$ blocks display two different arrangements as a function of the relative positions (sequence) of the *T* and *X* elements (Fig. 2). While the spatial distribution within the sheets is always a *XTTX* elemental block in the $ThCr_2Si_2$ type, alternating *XTTX* and *TXXT* sequences occur in the $CaBe_2Ge_2$ type. This atomic distribution generates Si–Si pairs in $ThCr_2Si_2$, whereas no Ge–Ge bonding occurs in one of the sheets in $CaBe_2Ge_2$.

The *XTTX* elemental block is characterized by a transition metal occupying the center of the $BaAl_4$ block, in tetrahedral *X* coordination, while the *TXXT* layer is characterized by a site inversion between the *T* and *X* elements. The *XTTX* elemental block is mainly encountered in the $ThCr_2Si_2$- and $TbFeSi_2$-type structures while the *TXXT* layer is encountered in the $CeNiSi_2$ and $NdRuSi_2$-type structures (Fig. 2). The relative stability of the *XTTX* and *TXXT* sequences, is one of the most intriguing problems encountered in the crystal chemistry of these layered compounds. According to Zheng and Hoffmann [34], the elemental RT_2X_2 block is characterized by different band dispersivity of the *T* and *X* sites, the more lattice dispersive site being the one that engenders more overlaps between equivalent sites, i.e. the separation between the equivalent sites is smaller than that of other sites. As shown in Fig. 2, in the *XTTX* block, the *T* metal occupies the more dispersive site while this site is occupied by the *X* element in the *TXXT* elemental block. This leads to important consequences for the relative stability of each block. Depending on the degree of band filling, the more electronegative atom will enter or avoid the more dispersive sites. Hence, for a *T* metal less electronegative than the *X* element and for a large band filling, the *XTTX* block will be more stable than the *TXXT* elemental block since the latter will have a higher Fermi energy. The numerous compounds crystallizing in the $ThCr_2Si_2$-type structure account for the great stability of the *XTTX* block. The stability of the $CaBe_2Ge_2$-type structure has been investigated by electronic structure

calculations by Zheng and Hoffmann [34]. According to this study, the occurrence of compounds with the $CaBe_2Ge_2$-type structure should be related to the *T*–*X* interlayer interactions between the *XTTX* and *TXXT* elemental blocks, favoring their simultaneous presence.

For the calculation of the electronic structure of $GdFe_xSi_2$ based on the LMTO method we have used an ordered and refined structural variant with the composition $GdFe_{0.5}Si_2$ in space group *Amm*2, a subgroup of *Cmcm*, to avoid the statistical occupation of the Fe site (Table 4). The structure contains zig-zag chains of Si(1) with Si–Si distances of 2.359 Å with terminally bonded Si(2) atoms, as shown in Fig. 3. Based on the Zintl concept formal oxidation states can be assigned resulting in a reasonable formula $Gd^{3+}(Fe^{2+})_{0.5}Si(1)^{1-}Si(2)^{3-}$. The DOS (density of states) curve indicates that $GdFe_{0.5}Si_2$ is a metal. The occupied Si states are distributed from –11 eV to the Fermi level, whereas the occupied Fe 3*d* states are located between –5 eV and 0 eV. The calculated COHP curves for the important interactions in $GdFe_{0.5}Si_2$ are shown in Fig. 3. There is a strong bonding interaction between the Fe and Si(2) atoms. The Fe–Si(1) interactions are very weak because of the large Fe–Si(1) distances and are therefore not shown in Fig. 4. Strong Si(1)–Si(1) and Si(2)–Si(1) interactions are found as expected from the analyses based on the Zintl concept (above) whereas the Si(2)–Si(2) interactions are negligibly small. The top valence electrons are all in bonding orbitals and any further filling with electrons, e.g. by additional Fe atoms, will lead to a significant occupation of antibonding states. As the *d* electron count increases across the first transition series, the electronegativity rises as well (1.55, 1.83, 1.88, 1.91 and 1.90 for Mn, Fe, Co, Ni and Cu, versus 1.9 for Si in Pauling scale). Not only the dispersivity favors the $CeNiSi_2$ structure (less electronegative atoms occupy the less dispersive sites), but also the *d* electrons start to fill the antibonding states above the Fermi level indicated in Fig. 3, thus any higher *d* electron count further favors the $CeNiSi_2$ structure.

Table 4: Atomic coordinates for $GdFe_{0.5}Si_2$ in the space group *Amm*2 with $a = 3.9527(6)$, $b = 4.0496(8)$, $c = 16.416(2)$.

Atom	Site	*x*	*y*	*z*	U_{eq}
Gd1	2*a*	0	0	0.6042(2)	0.0116(1)
Gd2	2*b*	1/2	0	0.39631(2)	0.007(1)
Fe[a]	2*a*	0	0	0.2525(2)	0.02(1)
Si1	2*a*	0	0	0.972(2)	0.02(1)
Si2	2*b*	1/2	0	0.049(3)	0.03(1)
Si3	2*a*	0	0	0.811(3)	0.01(1)
Si4	2*b*	1/2	0	0.183(2)	0.02(1)

[a]G (site occupancy) = 0.5.

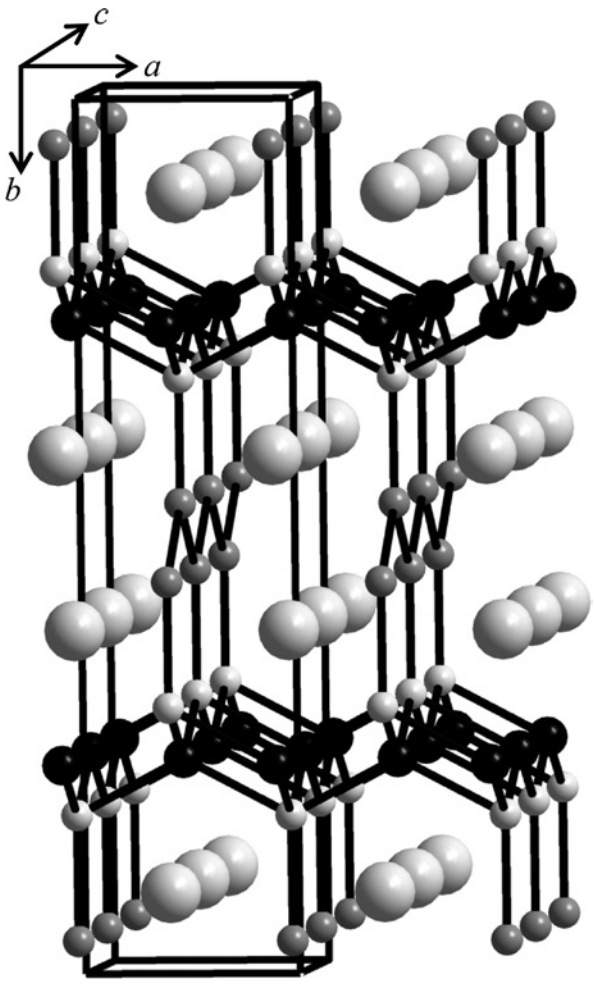

Fig. 3: Projection of the ordered variant of $GdFe_{0.5}Si_2$ in space group *Amm*2, see Table 4. Large gray circles correspond to Gd atoms, black ones to Fe atoms, medium and light gray spheres to Si(1) and Si(2) atoms, respectively.

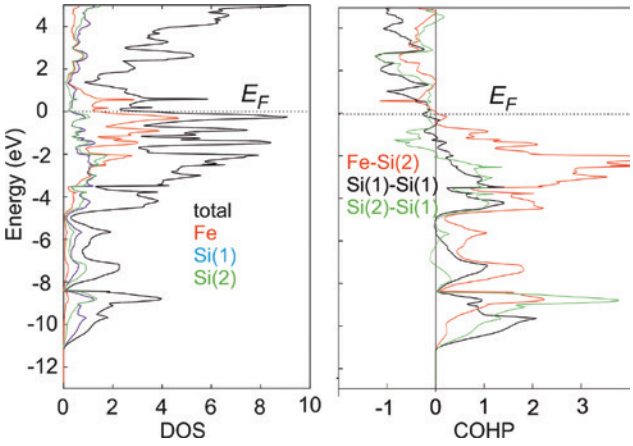

Fig. 4: Calculated total and projected Density of States (left) and cumulative COHP curves (right) for $GdFe_{0.5}Si_2$ in space group *Amm*2, see Table 4.

4 Conclusion

In summary, a new ternary silicide $GdFe_{1-x}Si_2$ ($x = 0.32$) has been synthesized from the elements by arc-melting. It crystallizes in space group *Cmmm* and represents a $TbFeSi_2$-type structure. The Fe position is not fully occupied and the structure refinement results in a composition $GdFe_{0.68}Si_2$ in agreement with a chemical analysis. The structure consists of zig-zag chains of Si(1) atoms which are terminally bound to additional Si(2) atoms. For an ordered variant of $GdFe_{0.5}Si_2$, the Zintl concept can be applied which results in formal oxidation states $Gd^{3+}(Fe^{2+})_{0.5}Si(1)^{1-}Si(2)^{3-}$. This assignment is confirmed by results of calculations based on the LMTO method, which also indicate that $GdFe_{0.5}Si_2$ is a metal. A more detailed computational analysis will be presented in a separate publication.

References

[1] O. I. Bodak, E. I. Gladyshevskii, *Sov. Phys. Crystallogr*. **1970**, *14*, 859.
[2] G. Venturini, B. Malaman, M. Meot-Meyer, D. Fruchart, G. Le Caer, D. Malterre, B, Roques, *Rev. Chim. Miner*. **1986**, *23*, 162.
[3] I. Ijjaali, G. Venturini, B. Malaman, *J. Alloys Compd*. **1999**, *282*, 153.
[4] N. M. Norlidah, G. Venturini, B. Malaman, *J. Alloys Compd*. **1998**, *268*, 193.
[5] V. I. Yarovets, Yu. K. Gorelenko, *Vestn. L'vovsk. Univ., Ser. Khim*. **1981**, *23*, 20.
[6] G. Venturini, M. N. Norlidah, B. Malaman, *J. Alloys Compd*. **1996**, *236*, 117.
[7] M. N. Norlidah, G. Venturini, E. Ressouche, B. Malaman, *J. Alloys Compd*. **1997**, *257*, 30.
[8] V. Mykhalichko, R. Gladyshenskii, *Chem. Chem. Technol.* **2016**, *10*, 1.
[9] L. Paccard, D. Paccard, J. Allemand, *J. Less-Common Met*. **1990**, *161*, 295.
[10] N. M. Norlidah, G. Venturini, B. Malaman, E. Ressouche, *J. Alloys Compd*. **1998**, *265*, 77.
[11] M. Norlidah, G. Venturini, B. Malaman, *J. Alloys Compd*. **1998**, *267*, 182.
[12] M. Francois, G. Venturini, B. Malaman, B. Roques, *J. Less-Common Met*. **1990**, *160*, 197.
[13] L. V. Krivulya, O. I. Bodak, Y. K. Gorelenko, *Inorg. Mater*. **1986**, *22*, 1685.
[14] B. Chabot, E. Parthé, J. Steinmetz, *J. Less-Common Met*. **1986**, *125*, 147.
[15] K. Cenzual, R. E. Gladyshevskii, E. Parthe, *Acta Crystallogr*. **1992**, *C48*, 225.
[16] R. Welter, G. Venturini, B. Malaman, *J. Alloys Compd*. **1992**, *185*, 235.
[17] B. I. Sapiev, O. L. Sologub, J. D. Seropegin, O. I. Bodak, P. S. Salamakha, *J. Less-Common Met.* **1991**, *175*, L1.
[18] V. Pavlyuk, O. Bodak, A. Sobolev, *Sov. Phys. Crystallogr*. **1991**, *36*, 493.
[19] O. I. Bodak, E. I. Gladyshevskii, V. I. Yarovets, V. M. Davydov, T. V. Il'chuk, *Inorg. Mater.* **1978**, *14*, 366.
[20] E. I. Gladyshevskii, O. I. Bodak, V. I. Yarovets, Yu. K. Gorelenko, R. V. Skolozdra, *Ukr. Fiz. Zh. (Russ. Ed.)*. **1978**, *23*, 77.
[21] J. Roger, V. Babizhetskyy, K. Hiebl, J.-F. Halet, R. Guérin, *J. Alloys Compd.* **2006**, *407*, 25.
[22] L. Akselrud, Y. Grin, WinCSD (version 4), Software Package for Crystallographic Calculations, Max-Planck-Institut für Chemische Physik fester Stoffe, Dresden (Germany) **2014**. See also: L. Akselrud, Y. Grin, *J. Appl. Crystallogr*. **2014**, *47*, 803.
[23] A. Altomare, M. C. Burla, M. Camalli, G. L. Cascarano, C. Giacovazzo, A. Guagliardi, A. G. G. Moliterni, G. Polidori, R. Spagna, *J. Appl. Crystallogr*. **1999**, *32*, 115.
[24] G. M. Sheldrick, *Acta Crystallogr.* **2015**, *C71*, 3.
[25] K. Brandenburg, Diamond (version 2.1c), Crystal and Molecular Structure Visualization, Crystal Impact - H. Putz & K. Brandenburg GbR, Bonn (Germany) **1999**.
[26] U. von Barth, L. Hedin, *J. Phys. C* **1972**, *5*, 1629.
[27] O. K. Andersen, *Phys. Rev. B* **1975**, *12*, 3060.
[28] O. K. Andersen, O. Jepsen, *Phys. Rev. Lett*. **1984**, *53*, 2571.
[29] O. K. Andersen, C. Arcangeli, R. W. Tank, T. Saha-Dasgupta, G. Krier, O. Jepsen, I. Dasgupta, *Mater. Res. Soc. Symp. Proc*. **1998**, *491*. 3.
[30] O. Jepsen, O. K. Andersen, The Stuttgart TB-LMTO-ASA programm (version 47), Max-Plank-Institut für Festkörperforschung, Stuttgart (Germany) **2000**.
[31] R. Dronskowski, P. E. Blöchl, *J. Phys. Chem*. **1993**, *97*, 8617.
[32] Z. Ban, M. Sikirica, *Acta Crystallogr*. **1965**, *18*, 594.
[33] B. Eisenmann, N. May, W. Müller, H. Schäfer, *Z. Naturforsch*. **1972**, *27b*, 1155.
[34] C. Zheng, R. Hoffmann, *J. Am. Chem. Soc*. **1986**, *108*, 3078.